Electronic Origin of Giant Magnetic Anisotropy in Multiferroic $LuFe_2O_4$

K.-T. Ko,[1] H.-J. Noh,[2,*] J.-Y. Kim,[3] B.-G. Park,[1,3] J.-H. Park,[1,4,3,†] A. Tanaka,[5] S. B. Kim,[6] C. L. Zhang,[7] and S-W. Cheong[6,7]

[1]*c_CCMR and Department of Physics, Pohang University of Science and Technology, Pohang 790-784, Korea*
[2]*Department of Physics, Chonnam National University, Gwangju 500-757, Korea*
[3]*Pohang Accelerator Laboratory, Pohang University of Science and Technology, Pohang 790-784, Korea*
[4]*Division of Advanced Materials Science, Pohang University of Science and Technology, Pohang 790-784, Korea*
[5]*Department of Quantum Matter, ADSM, Hiroshima University, Higashi-Hiroshima 739-8526, Japan*
[6]*l_PEM and Department of Physics, Pohang University of Science and Technology, Pohang 790-784, Korea*
[7]*R-CEM and Department of Physics and Astronomy, Rutgers University, Piscataway, New Jersey 08854, USA*

(Received 10 August 2009; published 12 November 2009)

We investigated the orbital anisotropy of $LuFe_2O_4$ using the Fe $L_{2,3}$- and O K-edge x-ray absorption spectroscopy (XAS) and cluster model calculations. X-ray magnetic circular dichroism reveals a surprisingly large orbital magnetic moment ($m_o \sim 0.8\mu_B$/f.u.), which originates the giant magnetic anisotropy. The polarization dependent XAS enables us to identify the orbital states and occupations, different from the band calculation predictions. These findings were examined by using the cluster model analysis, which also explains the orbital magnetic moment as well as the total moment ($2.9\mu_B$/f.u.). Taking into account the charge order, we also determined the spin structure.

DOI: 10.1103/PhysRevLett.103.207202 PACS numbers: 75.50.Gg, 75.30.Gw, 77.80.−e, 78.70.Dm

Since the discovery of intriguing coupled phenomena between magnetism and ferroelectricity in manganese oxides [1], multiferroicity has been intensively studied for its scientific interest and potential technological applications. Recent studies have shown that multiferroicity originates from various kinds of couplings between charge-spin-orbital-lattice degrees of freedom [2–4]. $LuFe_2O_4$ is the first iron-based multiferroic system with a charge order, which is coupled with the spin degree of freedom [5], and exhibits interesting properties such as giant magnetic coercivity [6], a magnetodielectric response [7], strong insulating behavior with a large band gap [8], etc. Although the spin and charge ordering patterns are naturally considered as key factors of the underlying physics, the exact patterns as well as the physical mechanisms are still under debate in both theory and experiment [8–11].

$LuFe_2O_4$ is crystallized in a layered hexagonal structure as shown in Fig. 1(a). The unit cell consists of three Fe double layers with 2.5+ average nominal valence (1:1 Fe^{2+} and Fe^{3+} ratio). A three dimensional charge order develops at $T_{CO} \simeq 320$ K [11,12] upon cooling, and magnetic spins are ordered ferrimagnetically along the c axis below $T_C \simeq 240$ K [6,10]. Such sequential charge and spin ordering in the triangular lattice is essential for the multiferroic properties since charge and spin orders are frustrated structurally and a polar charged state is stabilized as shown in Fig. 1(b); each double layer is divided into an Fe^{2+} and an Fe^{3+} rich layer in which the rare Fe^{3+} and Fe^{2+} ions locate at the center of the Fe^{2+} and Fe^{3+} honeycombs, respectively. The ground state is antiferroelectric with the $\vec{q} = (\frac{1}{3}\ \frac{1}{3}\ \frac{3}{2})$ charge order [11] while the electric field cooling drives the system to be ferroelectric as presented in Fig. 1(c). The electric polarization increases with development of the magnetic order [5], resulting in a giant magnetodielectric response [7].

Theoretical explanations were proposed for the antiferroelectric and ferroelectric charge orders [9,11] and the magnetodielectric effect was explained to be due to suppression of charge fluctuation [9]. However, the detailed spin structure is still unknown, and the microscopic view is obscured by the complex coupling of spin and charge orders. A possible spin configuration was suggested based on the neutron diffraction [10] and the Monte Carlo simulation [13], but both studies could not determine the site specific spin structure. On the other hand, $LuFe_2O_4$ exhibits extreme magnetic properties: a giant magnetic anisot-

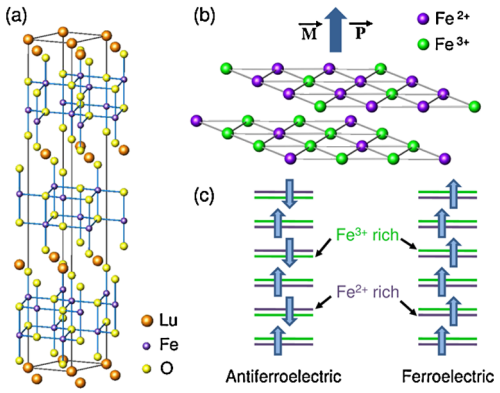

FIG. 1 (color online). (a) Crystal structure of $LuFe_2O_4$ with Fe double layers and Lu layers. (b) Fe^{2+} rich (2:1 Fe^{2+}/Fe^{3+} ratio) and Fe^{3+} rich (2:1 Fe^{3+}/Fe^{2+} ratio) double layer with the charge order. The electric polarization (≤ 320 K) and the magnetization (≤ 240 K) are parallel to the c axis. (c) Schematic diagrams of two different charge orders.

ropy of over 70 T [14] and a huge magnetic coercivity of ~10 T [6]. These magnetic behaviors were attributed to the formation of Ising pancakelike domains [14], but their microscopic origin has not been understood, yet.

In this Letter, we investigated the orbital anisotropy and spin configuration of $LuFe_2O_4$ using the x-ray absorption spectroscopy (XAS) and x-ray magnetic circular dichroism (XMCD). The polarization dependent XAS enables us to explore the local electronic structure including the orbital occupations. On the other hand, XMCD gives quantitative information on the spin and orbital magnetic moments. Combined study of XAS and XMCD not only shows that the system has a large orbital magnetic moment induced by the orbital anisotropy, but also determines the spin structure.

The XAS and XMCD measurements were performed at the 2A elliptically polarized undulator beam line in the Pohang Light Source. Stoichiometric $LuFe_2O_4$ single crystals grown by the floating zone method [14] were cleaved *in situ* in ultrahigh vacuum better than 5×10^{-10} Torr. The polarization dependent XAS spectra were obtained at 250 K with more than 98% linearly polarized light at 70° beam incidence to the surface normal (hexagonal c axis), which yields near $\vec{E} \parallel \vec{c}$ or $\vec{E} \perp \vec{c}$ without change of the experimental geometry by utilizing the planar or vertical polarization selectivity of the elliptically polarized undulator, respectively. The XMCD spectra were measured with ~95% circularly polarized light at 220 K. A 0.8 T electromagnet was used to align the magnetic moments along the c axis and the photon incident angle is 22.5° off from the c axis. All the spectra were obtained in total electron yield mode and the mesh current was simultaneously recorded for normalization. The cluster model calculation including the full ionic multiplets and configuration interactions, often called the configuration-interaction (CI) calculation [15], was performed for the FeO_5 bipyramid, and the Fe-O distances [16] were taken into account.

The Fe L-edge XMCD results of $LuFe_2O_4$ are presented in Fig. 2. The absorption spectra ρ_+ and ρ_-, which were collected for the respective magnetization $\vec{M}$ parallel and antiparallel to the photon helicity vector, are roughly divided into the L_3 and L_2 regions due to the large core-hole spin-orbit coupling energy. The spectral feature in the L_3 region is represented by prominent two peaks corresponding to the Fe^{2+} and Fe^{3+} white lines [17]. The dichroism signal $\Delta\rho$ displays ferrimagnetic features; $\Delta\rho$ is negative and positive at the Fe^{2+} and Fe^{3+} peak regions, respectively, and the negative weight is larger than the positive one. These features mean that the net Fe^{2+} magnetic moment is parallel while the net Fe^{3+} moment is antiparallel to the total net magnetization $\vec{M}$. The spin value of Fe^{2+} ($S = 2$) is smaller than that of Fe^{3+} ($S = 5/2$), and thus the smaller positive weight for Fe^{3+} implies that all Fe^{3+} spins are not aligned to be antiparallel to the total net moment. Considering that the magnetic unit cell formed by triple formula units in the hexagonal structure has three Fe^{2+} and

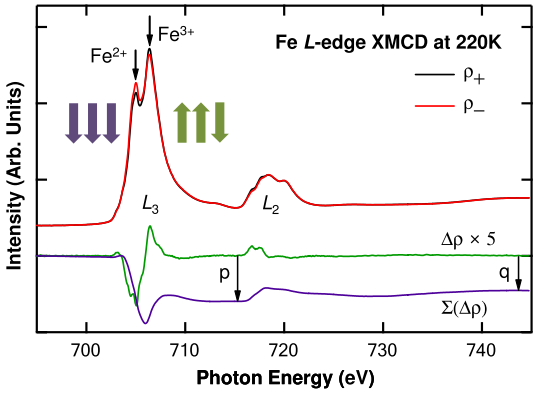

FIG. 2 (color online). Fe $L_{2,3}$-edge XMCD spectra of $LuFe_2O_4$ at 220 K. Fe^{2+} and Fe^{3+} white lines in the L_3 region are indicated by arrows. The dichroism spectrum, $\Delta\rho = \rho_+ - \rho_-$, is obtained from the difference of the absorption spectra. The bold arrows represent the ferrimagnetic spin configuration in the tripled unit cell.

Fe^{3+} ions, one can naturally conclude that one Fe^{3+} spin is parallel and the other two spins are antiparallel to $\vec{M}$ while all three Fe^{2+} spins are parallel to $\vec{M}$. This peculiar spin alignment yields the total spin magnetic moment of $2.33\mu_B$/f.u. in the simple ionic limit ($4\mu_B$ for Fe^{2+} and $5\mu_B$ for Fe^{3+}). This value is somewhat away from the observed saturation moment $2.9\mu_B$/f.u., which was previously explained in terms of a model of the $Fe^{2.5+}$ ($4.5\mu_B$) mixed valence state with a 2:1 ratio ferrimagnetic spin alignment yielding $3\mu_B$/f.u. [6,10]. This model, however, is not compatible to the XMCD results.

The large difference between the net spin moment ($2.33\mu_B$) and the saturation moment ($2.9\mu_B$) can be explained with an extremely large unquenched orbital magnetic moment m_o, which is generally quenched by the crystal field [18]. XMCD is a unique tool to explore m_o [19]. As can be seen in Fig. 2, the integration $\sum(\Delta\rho)$ of the dichroism signal over the entire $L_{2,3}$ region, which is proportional to m_o, indeed gives a considerably large value, meaning that a large m_o survives in this system. Although the measurement was performed at relatively high temperature to avoid the charging effect in this insulating $LuFe_2O_4$ and the ordered moment is greatly reduced from the full moment at 4 K [20], we can still extract the orbital to spin moment ratio from the XMCD result [21]. Taking $p = -0.12$ and $q = -0.09$, the ratio is estimated to be $m_o/m_s = 0.34$ [22] by using the sum rule, and the ionic net spin moment $m_s = 2.33\mu_B$/f.u. leads to $m_o = 0.79 \pm 0.05\mu_B$/f.u. The negative q value designates that the orbital momentum is parallel to the spin momentum, consistent with the fact of the more than half full, and the total moment is estimated to be $3.12\mu_B$/f.u.. This ionic value will be slightly reduced with the degree of covalency and become very close to the saturation moment discussed far below. The XMCD results verify that $LuFe_2O_4$ has an extremely large m_o. This large m_o contributes a huge magnetic anisotropy energy, $-\xi\Delta\boldsymbol{L}\cdot\boldsymbol{S}$ [23], of a few

tens meV, which is very consistent with the observed giant magnetic anisotropy, leading to an Ising ferrimagnet with the gigantic coercivity [14].

The origin of the large orbital moment can be found in the electronic structure with strong orbital anisotropy. Figure 3(a) shows the polarization dependent O K-edge XAS spectra compared with the cluster model calculation results. The spectra reflect the unoccupied conduction bands due to the hybridization with the O $2p$ states. The full range spectra presented in the inset display three prominent features in the 530–550 eV region, which correspond to the Fe^{3+} $3d$, Fe^{2+} $3d$, and Lu $5d/6sp$/Fe $4sp$ states as denoted in the figure, respectively. Here we focus on the Fe $3d$ region, which mainly determines the physical properties. The spectra in the Fe^{3+} region show nearly the same peak structures as those in the Fe^{2+} region. Under the FeO_5 bipyramid crystal field, the Fe $3d$ level split into two doublets, e_g'' (d_{zx}, d_{yz}) and e_g' (d_{xy}, $d_{x^2-y^2}$), and a singlet, $a_{1g}(d_{3z^2-r^2})$ [18]. The strict dipole selection rule of the polarization dependent XAS enables us to identify the orbital states. The e_g' in-plane orbital states are exclusively hybridized with the in-plane O $2p_{x,y}$ states, and thus can be reached in the absorption process for the polarization vector $\vec{E} \parallel \vec{ab}$, while the out-of-plane a_{1g} orbital state is mainly accessed for $\vec{E} \parallel \vec{c}$. Taking advantage of the selection rule, we can confidently assign e_g'', e_g', and a_{1g} states indicated in the figure. The O K-edge XAS verifies the orbital energy level structure with the e_g'' lowest, different from the previous band calculation, which predicted more occupation in the e_g' state [9,24].

The XAS spectra in details can be explained by the cluster model (CI) calculation for the FeO_5 bipyramid [25]. As shown in the figure, all the spectral features are well reproduced for both $\vec{E} \parallel \vec{ab}$ and $\vec{E} \parallel \vec{c}$. The e_g'' and e_g' energy levels under the bare crystal field become reversed due to the difference in the hybridization strengths with the O $2p$, and the e_g'' state becomes the lowest as depicted in Fig. 3(b). With the aforementioned electronic structure, the unquenched large orbital moment m_o can be explained as follows. In Fe^{2+} (d^6), an extra minority spin electron occupies the lowest doublet, e_g'' (d_{zx}, d_{yz}). The degenerate $d_{yz} = \frac{i}{\sqrt{2}}(\phi_{3d1} + \phi_{3d-1})$ and $d_{zx} = \frac{-1}{\sqrt{2}}(\phi_{3d1} - \phi_{3d-1})$ becomes split into $m_l = 1$ and -1 states by the spin-orbit coupling, resulting in the unquenched large m_o. Indeed the ground state in the CI calculation exposes a large $m_o = 0.81\mu_B$ for Fe^{2+}, consistent with the XMCD result. The spin moment is obtained to be $4.50\mu_B$ for Fe^{3+} and $3.67\mu_B$ for Fe^{2+}, yielding the net spin moment $2.17\mu_B$/f.u. in the ferrimagnetic spin order obtained in the XMCD study. This value is slightly reduced from the ionic value $2.33\mu_B$/f.u. due to the configuration mixing, and the total magnetic moment becomes $2.98\mu_B$/f.u. in a good agreement with the reported saturation moment $2.9\mu_B$/f.u. [5,14].

Now let us discuss the spin structure. The spin structure in the charge ordered double layer has been investigated in various approaches such as group theoretical analysis, neutron diffraction, and Monte Carlo simulation [10,13], but none of the studies provided a conclusive spin structure. As discussed in the XMCD results, all the Fe^{2+} spins are aligned ferromagnetically, probably due to the large orbital moment of Fe^{2+} contributing a strong uniaxial magnetic anisotropy. On the other hand, the orbital moment in the half-filled Fe^{3+} is negligible, and the spin alignment, which could be determined by the competition between the Fe^{2+}-Fe^{3+} double exchange and the Fe^{3+}-Fe^{3+} superexchange interactions in the magnetically frustrated triangular lattice, results in the 1:2 ferrimagnetic spin order; one Fe^{3+} spin is parallel and the other two spins are antiparallel to the ferromagnetic Fe^{2+} spin. These spin alignments topologically allow only two possibilities for the spin structure in the Fe^{2+}-Fe^{3+} charge ordered hexagonal double layer structure as shown in Fig. 4: the parallel Fe^{3+} spin either in the Fe^{3+} rich plane [Fig. 4(a)] or in the Fe^{2+} rich plane [Fig. 4(b)].

The XMCD spectra for the two spin structures were simulated with the CI calculations, in which the site difference is taken into account. It should be noticed that the Fe^{2+} and Fe^{3+} rich layers have different charge environments, which contribute differences in the Madelung potential at the Fe sites and energy shifts in the absorption energies [26]. As shown in the figure, the calculated XMCD spectrum well reproduces the complicated line shape of the experimental one in the spin structure with the parallel Fe^{3+} spin in the Fe^{3+} rich layer [Fig. 4(a)] while the agreement between the calculation and the experiment becomes much worse in the other spin structure

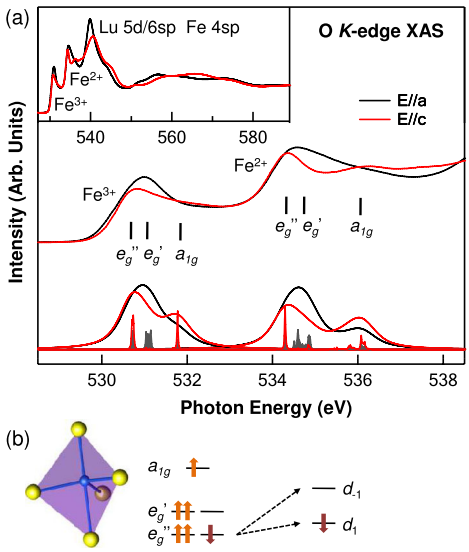

FIG. 3 (color online). (a) Polarization dependent O K-edge XAS spectra (top) of $LuFe_2O_4$ at 250 K are compared with the CI calculation results (bottom). The wide range spectra are presented in the inset. The e_g', e_g'', and a_{1g} orbital states under the FeO_5 crystal field are identified. (b) Schematic crystal field splitting. The lowest e_g'' (d_{zx}/d_{yz}) doublet is split into $m_l = 1$ and -1 states by the spin-orbit coupling.

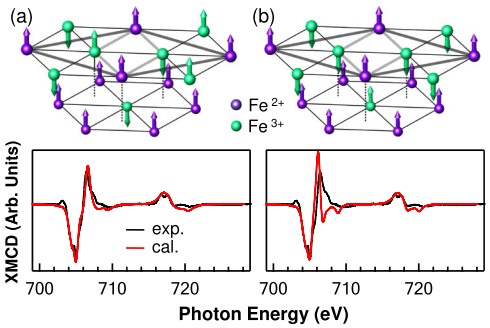

FIG. 4 (color online). CI calculations for the XMCD spectra for the two spin structure, in which the $\sqrt{3} \times \sqrt{3}$ magnetic unit cell is indicated with solid thick lines; (a) antiparallel and (b) parallel Fe^{3+} spin configurations in Fe^{3+} rich layer.

[Fig. 4(b)]. Indeed, the Mössbauer study reported that there exist three distinguishable Fe^{3+} sites and concluded the antiparallel Fe^{3+} spin alignment in the Fe^{3+} rich layer [27], consistent with the former spin structure: one Fe^{3+} in the Fe^{2+} rich layer and two with different spin directions in the Fe^{3+} rich layer. Moreover, it is expected to show the same diffraction pattern observed in the neutron study [10] if the Fe^{2+} and Fe^{3+} spins are replaced with the average $Fe^{2.5+}$ spins. The formation of the spin structure can simply be understood in terms of the antiferromagnetic superexchange interactions in the different Fe^{3+}-O-Fe^{3+} bond angles. The bonding angle for the interlayer neighboring Fe^{3+} ions is 97°, which is close to 90°, and thus the superexchange interaction is not large enough to dominate the magnetic coupling. On the other hand, neighboring Fe^{3+} ions in the Fe^{3+} rich plane is 118°, a relatively larger angle, so that the interaction stabilizes the antiferromagnetic coupling, as also pointed out by the Monte Carlo simulation [13].

In summary, we investigated the orbital anisotropy and spin configuration of the multiferroic $LuFe_2O_4$ using the x-ray absorption spectroscopy with circular and linear dichroism at the Fe $L_{2,3}$ edge and O K edge. The XMCD showed that the system has the large unquenched orbital magnetic moment, which originates the giant magnetic anisotropy and coercivity, and also suggested a peculiar ferrimagnetic alignment of the Fe^{2+} and Fe^{3+} spins. In the polarization dependent XAS, the lowest energy orbital state is identified as $e_g''(zx, xy)$, which becomes split by the spin-orbit coupling and results in the large orbital moment at the Fe^{2+} sites. The observations as well as the total magnetic moment were well described in the cluster model analysis, which also enables us to finalize the site specific spin structure.

This work was supported by the National Creative Initiative Center for Cross-coupled Complex Materials Research and WCU program (R31-2008-000-10059-0). H.-J. Noh acknowledges the support of the NRF Grant No. 2007-00758. The work at Rutgers was supported by the DOE Grants No. DE-FG02-07ER46382. PAL is supported by POSTECH and MOEST.

*ffnhj@chonnam.ac.kr
†jhp@postech.ac.kr

[1] T. Kimura *et al.*, Nature (London) **426**, 55 (2003); N. Hur *et al.*, *ibid.* **429**, 392 (2004).
[2] D. I. Khomskii, J. Magn. Magn. Mater. **306**, 1 (2006).
[3] S-W. Cheong and M. Mostovoy, Nature Mater. **6**, 13 (2007).
[4] J. van den Brink and D. I. Khomskii, J. Phys. Condens. Matter **20**, 434217 (2008).
[5] N. Ikeda *et al.*, Nature (London) **436**, 1136 (2005).
[6] J. Iida *et al.*, J. Phys. Soc. Jpn. **62**, 1723 (1993).
[7] M. A. Subramanian *et al.*, Adv. Mater. **18**, 1737 (2006).
[8] X. S. Xu *et al.*, Phys. Rev. Lett. **101**, 227602 (2008).
[9] H. J. Xiang and M.-H. Whangbo, Phys. Rev. Lett. **98**, 246403 (2007).
[10] A. D. Christianson *et al.*, Phys. Rev. Lett. **100**, 107601 (2008).
[11] M. Angst *et al.*, Phys. Rev. Lett. **101**, 227601 (2008).
[12] Y. Yamada, K. Kitsuda, S. Nohdo, and N. Ikeda, Phys. Rev. B **62**, 12167 (2000).
[13] M. Naka, A. Nagano, and S. Ishihara, Phys. Rev. B **77**, 224441 (2008).
[14] W. Wu *et al.*, Phys. Rev. Lett. **101**, 137203 (2008).
[15] A. Tanaka and T. Jo, J. Phys. Soc. Jpn. **63**, 2788 (1994).
[16] M. Isobe *et al.*, Acta Crystallogr. Sect. C **46**, 1917 (1990).
[17] B.-G. Park *et al.*, Phys. Rev. B **79**, 035105 (2009).
[18] D.-Y. Cho *et al.*, Phys. Rev. Lett. **98**, 217601 (2007); D.-Y. Cho *et al.*, Phys. Rev. B **79**, 035116 (2009).
[19] B. T. Thole, P. Carra, F. Sette, and G. van der Laan, Phys. Rev. Lett. **68**, 1943 (1992); C. T. Chen *et al.*, *ibid.* **75**, 152 (1995).
[20] The total moment estimated from XMCD at 220 K is $0.24 \pm 0.03 \mu_B$/f.u. and is consistent with the saturated moment $0.25 \mu_B$/f.u. obtained from SQUID measurements.
[21] J.-Y. Kim, T. Y. Koo, and J.-H. Park, Phys. Rev. Lett. **96**, 047205 (2006).
[22] As the quadrupole contribution is taken into account, the ratio increases by about 13% to become 0.38.
[23] The in-plane orbital moment is estimated to be $0.3 \mu_B$/f.u. at 75 T in the cluster calculation, which gives $\Delta \boldsymbol{L} \simeq 0.5 \mu_B$/f.u..
[24] A. Nagano, M. Naka, J. Nasu, and S. Ishihara, Phys. Rev. Lett. **99**, 217202 (2007).
[25] The calculations were performed for $d^n \oplus d^{n+1}\underline{L} \oplus d^{n+2}\underline{L}^2$ with $U_{dd} = 6.5$ eV, $\Delta = 6.0$ eV for Fe^{2+}, $U_{dd} = 5.5$ eV, $\Delta = 4.0$ eV for Fe^{3+}, and $V_{pd\sigma}(z^2) = 3.4$ eV. Slater integrals were taken to be ~60% of the atomic values.
[26] Numerical calculation in the ionic lattice gives that both Madelung potentials at the Fe^{2+} and Fe^{3+} sites are higher in the Fe^{3+} rich layer than respective ones in the Fe^{2+} rich layer. The different charge environment is also expected to slightly reduce the absorption energy at the Fe site in the Fe^{3+} rich layer. The best fit was obtained for the energy shifts of 0.7 and 0.4 eV for Fe^{2+} and Fe^{3+}, respectively. The details will be published elsewhere.
[27] M. Tanaka *et al.*, J. Phys. Soc. Jpn. **58**, 1433 (1989); B. K. Bang *et al.*, Phys. Status Solidi B **244**, 4566 (2007).